Journal of Composites and Compounds 7(2025) 1-10

Available Online at www.jourcc.com

Journal homepage: www.JOURCC.com

Journal of Composites and Compounds

Copper bismuth oxide ($CuBi_2O_4$): Synthesis, properties and potential applications

Saifullahi Shehu Imam *

Department of Pure and Industrial Chemistry, Bayero University P.M.B 3011, Kano, Nigeria

ABSTRACT

Copper bismuth oxide ($CuBi_2O_4$) is a p-type semiconductor which is an outstanding representative of the spinel-type compounds. In the present article, various methods used for the synthesis of $CuBi_2O_4$ such as hydrothermal, co-precipitation, microwave-assisted, mechanochemical, solid-state etc. with the feature(s) of the product obtained have been summarized. Furthermore, the promising potential applications of $CuBi_2O_4$ such as in gas sensing, as a photocatalyst, as a photocathode material, in activating certain oxidants such as peroxymonosulfate and H_2O_2, and for various other applications have also been reviewed. Such compiled study will be useful to specialists dealing with $CuBi_2O_4$ and is also expected to promote the further application of $CuBi_2O_4$.

Peer review under responsibility of UGPH.

ARTICLE INFORMATION

Article History:
Received 8 June 2024
Received in revised form 12 November 2024
Accepted 23 February 2025

Keywords:
$CuBi_2O_4$
Synthesis
Hydrothermal
Photocatalyst
Band-gap

1. Introduction

$CuBi_2O_4$ (Fig. 1) is a unique representative of the spinel-type compounds with the general formular AB_2O_4, where A represents a divalent metal cation and B represents a trivalent metal cation [1]. It is a P-type semiconductor with interesting physicochemical properties such as high-temperature heat capacity, magneticity, electrochemical capacitance, dielectricity, catalysis, and photoelectrochemical property [2].

The tetragonal $CuBi_2O_4$ has a crystal structure with a three-dimensional array of $[CuO_4]^{6-}$ square-planar units, staggered along the c-axis and separated by Bi^{3+} ions [3]. The conduction band position of $CuBi_2O_4$ is (−0.6 to −0.4 eV vs. SHE), indicating that it has strong reduction potential [4]. Multiphonon hopping of charge carriers and the weak electron-phonon coupling govern the electrical properties of $CuBi_2O_4$ [5].

$CuBi_2O_4$ has a band gap of 1.5 – 1.8 eV, which makes it able to harness a significant portion of the visible light from the solar spectrum [7, 8].

It has excellent photostability, large light penetration depth and good photocatalytic performance [9]. $CuBi_2O_4$ possess a 0.225 V positive surface photovoltage when irradiated with photons of energy $h\nu > 1.8$ eV, indicating holes as majority charge carriers, which is consistent with its p-type behaviour [10]. Although, due to the lack of chemical affinity with water matrix, mismatched band positions, recombination of the photogenerated charge carriers, high photostability, insufficient quantum yields, the performance of pristine $CuBi_2O_4$ is still not satisfactory [11]. Nevertheless, $CuBi_2O_4$ has been used as photocatalytic material [12], negative electrodes in lithium-ion batteries [13], and in gas sensing [14].

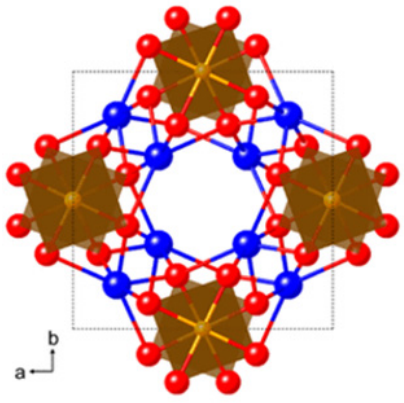

Fig. 1. $CuBi_2O_4$ crystal structure as viewed along the c-axis. Bi, Cu, and O atoms are represented by blue, orange, and red spheres, respectively. Image reproduced with permission from Ref. [6].

Due to the aforementioned features and applications of $CuBi_2O_4$, it is necessary to summarize research results on $CuBi_2O_4$. This article summarized the recent research progress in $CuBi_2O_4$. In doing that, emphasis has been placed on the properties and practical applications of $CuBi_2O_4$ from various perspectives, in addition to adequate discussion on the frequent methods employed.

* *Corresponding author: Saifullahi Shehu Imam. Email: ssimam.chm@buk.edu.ng*
https://doi.org/10.61186/jcc.7.1.1

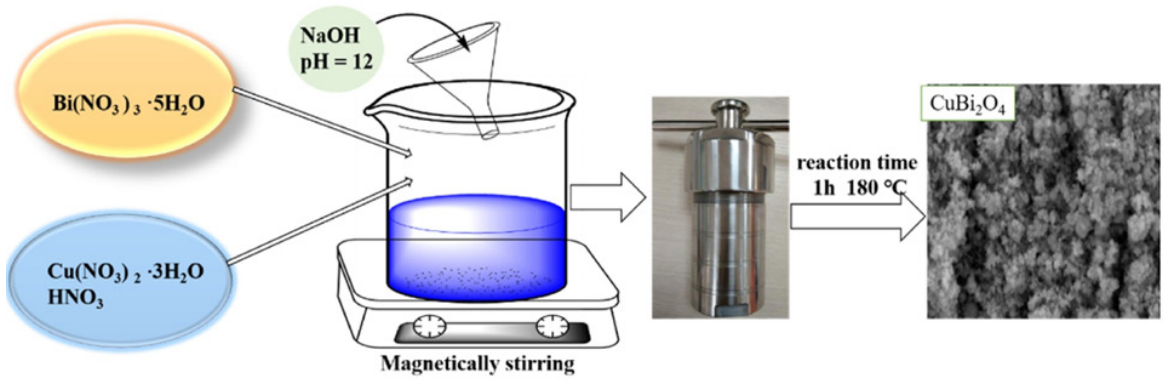

Scheme 1. Hydrothermal preparation of $CuBi_2O_4$. Reproduced with permission from [18].

2. Synthesis of copper bismuth oxide

Various methods including solid-state [15], drop-casting [6], co-precipitation [12], hydrothermal [16], mechanochemical [4], microwave-assisted hydrothermal [17] etc. as summarized in Table 1 have been reported for the synthesis of $CuBi_2O_4$. Among these methods, the hydrothermal synthesis is frequently reported and a typical representation of hydrothermal method as employed by Zhang et al. [18] to synthesize $CuBi_2O_4$ is shown in Scheme 1.

A number of synthesis parameters were found to have impact on the features of the $CuBi_2O_4$ end-product and have been studied by some researchers. For instance, Gao et al. [12] studied the effect of reaction time on the co-precipitation synthesis of $CuBi_2O_4$. The samples were synthesized by varying the reaction time from 0.5 - 12 h. In the case of the XRD results (Fig.2), samples synthesized at 0.5 and 1 h still contain mixture of phases. However, pure tetragonal phase of $CuBi_2O_4$ was formed at 3 h and longer reaction times. Never the less, the reaction time had clear impact on the morphology (Fig. 3).

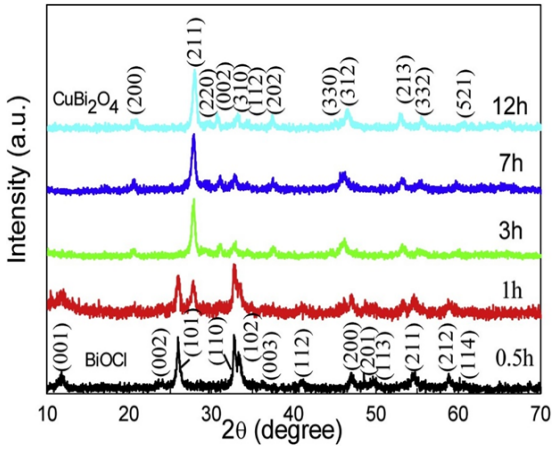

Fig. 2. XRD patterns of $CuBi_2O_4$ samples obtained at different reaction times. Reproduced with permission from [12].

The effects of treatment time (6 – 24 h), Cu $(NO)_2$ to NaOH molar ratios (1:30 and 1:10), and Cu^{2+} concentrations (0.02 M and 0.2 M) on the hydrothermal synthesis of $CuBi_2O_4$ have been studied by Xie et al. [16]. In Fig.4 , XRD patterns and SEM images of the samples prepared at 120 °C for 6 h (labelled as sample A), 12 h (labelled as sample B, D, E, F) and 24 h (labelled as sample C) with $Cu(NO_3)_2$ to NaOH molar ratios of 1:30 (A, B, C, D) and 1:10 (E, F) and Cu^{2+} concentrations of 0.02 M (A, B, C, E) and 0.2 M (D, F). The influence of treatment time and Cu^{2+} concentration is insignificant on the lattice orientation and crystallinity. However, samples prepared at 6, 12, and 24 h have similar leaf-like, two-dimensional nanosheet morphology (SEM images A, B, C). The average crystallite sizes for samples prepared at 6, 12, and 24 h were 200, 400, 500 nm in width and 400, 700, 800 nm in length. The samples synthesized using Cu^{2+} concentrations of 0.2 M (SEM image D) and 0.02 M (SEM image E) have agglomerated nanorods morphology.

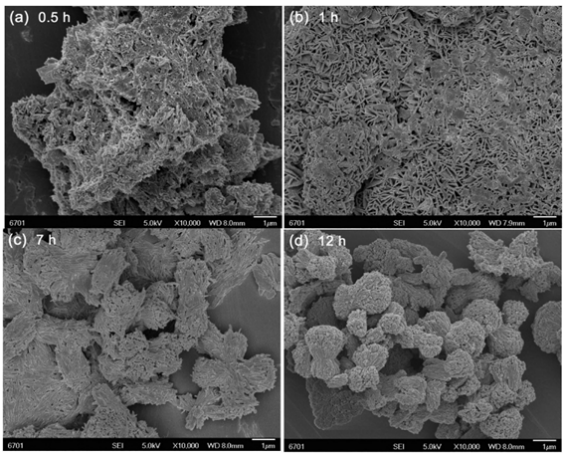

Fig. 3. SEM images of $CuBi_2O_4$ samples obtained at different reaction times. (a) 0.5 h; (b) 1 h; (c) 7 h; (d) 12 h. Reproduced with permission from [12].

In a different study, Ribeiro et al. [17] reported the rapid microwave-assisted hydrothermal synthesis of $CuBi_2O_4$. During the process, the $CuBi_2O_4$ was synthesized at different times (8 min, 16 min, and 32 min). Based on the FESEM image presented in Fig. 5, $CuBi_2O_4$ produced using 8 min reaction time were dominantly coral-shaped particles, and become spheres composed of nanorods with longer treatment time. However, there was no significant change in morphology for $CuBi_2O_4$ synthesized using hydrothermal treatments of 16 and 32 min. On the other hand, the effect of reaction time on the morphology of $CuBi_2O_4$ synthesized by Abdulkarem et al. [19] was found to be different. During the synthesis, agglomerated particles were formed at a reaction time of 2 h. As the reaction time increases, the nanoparticles coherently assembled into microrods. When the reaction time was extended to 12 h, the microrod split into bundled nanorods and some particles appeared on their surface (Fig. 6).

The effect of cupric acetate concentration on the synthesis of $CuBi_2O_4$ was studied by Abdulkarem et al. [19]. They observed that, high concentration of cupric acetate resulted in the formation of irregular $CuBi_2O_4$ nanoparticles. However, as the concentration decreases, the particles began to agglomerate to form short rods, and with further decrease in concentration, nanorod morphology was completely formed (Fig. 7).

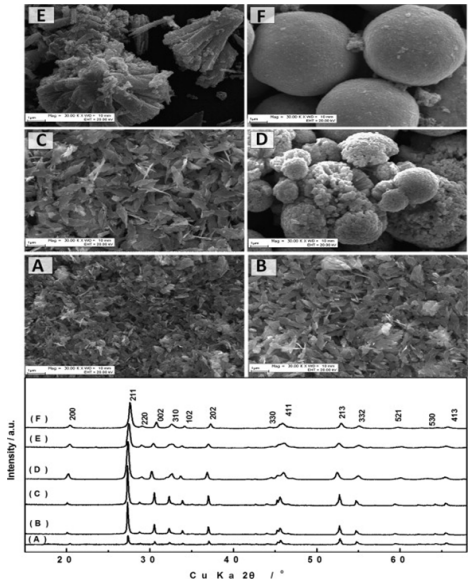

Fig. 4. XRD patterns and SEM images of the samples prepared at 120 °C for 6 (A), 12 (B, D, E, F) and 24 h (C) with the $Cu(NO_3)_2$-to-NaOH molar ratios of 1:30 (A, B, C, D) and 1:10 (E, F) and Cu^{2+} concentrations of 0.02 M (A, B, C, E) and 0.2 M (D, F) Reproduced with permission from [16].

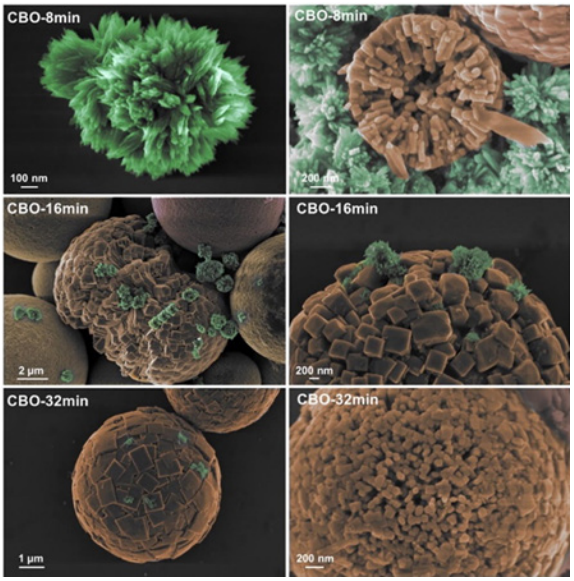

Fig. 5. FESEM micrographs of $CuBi_2O_4$ at different times of synthesis. Reproduced with permission from [17].

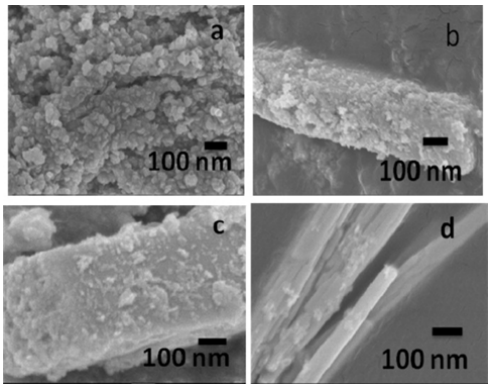

Fig. 6. SEM images of samples prepared with 0.030 M cupric acetate for (a) 2 h, (b) 4 h, (c) 8 h and 12 h (d). Reproduced with permission from [19].

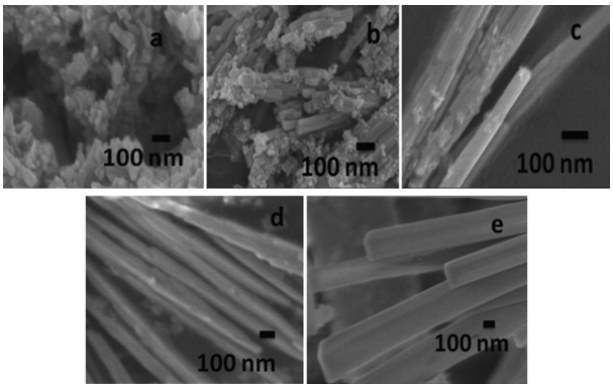

Fig. 7. SEM images of $CuBi_2O_4$ synthesized using cupric acetate concentration of (a) 0.061 M, (b) 0.036 M, (c) 0.030 M, (d) 0.024 M, and (e) 0.018 M. Reproduced with permission from [19].

Table 1
Several synthesis methods to prepare pristine $CuBi_2O_4$ with its feature(s).

No.	Method	Reaction conditions	Feature(s)	Ref.
1.	Hydrothermal	4.8507 g Bi $(NO_3)_3$ and 1.2080 g Cu $(NO_3)_2$ were dissolved in 20 mL of 0.1 mol/L nitric acid solution. 20 mL of 1.25 mol L^{-1} aqueous sodium hydroxide solution was dropped into this solution under vigorous stirring. The mixture was transferred into a 50 mL Teflon-sealed autoclave and the autoclave maintained at 150 °C for 24 h. The resultant precipitate was collected by centrifugation and thoroughly washed with deionized water (three times) and absolute ethanol (two times). Dried at 60 °C for 8 h.	Particles with slightly agglomerated morphology and average diameter of 60 nm. Band gap of 1.48 eV.	[20]
2.	Hydrothermal	2.42 g Bi $(NO_3)_3$ $5H_2O$, 0.6 g Cu $(NO_3)_3$ $3H_2O$ and 0.87 g NaOH were mixed into 80 mL deionized water and stirred for 3 h. Resulted slurry was transferred into a 100 mL Teflon-lined stainless-steel autoclave, and then heated at 180 °C for 24 h. Formed powders were washed with distilled water for three times and finally dried at 70 °C in the oven.	Smooth-faced microrods with the diameter of 200 nm and 4 μm in length. Band gap of 1.76 eV.	[9]
3.	Hydrothermal	5 mmol of Bi $(NO_3)_3 \cdot 5H_2O$ was dissolved in 60 mL deionized (DI) water. 2.5 mmol of Cu $(NO_3)_3 \cdot 3H_2O$ was mixed into the above suspension under vigorously stirring until Cu $(NO_3)_3 \cdot 3H_2O$ was completely dissolved.	Microspheres structure consisting of nanorods. Band gap of 1.73 eV.	[21]

No.	Method	Reaction conditions	Feature(s)	Ref.
		20 mL of 1 M NaOH was added to above mixture and stirred continuously for 3 h. The mixture was then poured into a 100 mL Teflon-lined steel autoclave to conduct a hydrothermal procedure at 180 °C for 18 h. Product was washed with DI water and ethanol for several times and dried at 60 °C.		
4.	Hydrothermal	2.42 g of Bi $(NO_3)_3{\cdot}5H_2O$, 0.6 g Cu $(NO_3)_2{\cdot}2.5H_2O$ and 0.87 g NaOH were mixed in 80 mL of distilled water and stirred for 3 h. Homogeneous precursor was then transferred into 100 mL Teflon-lined stainless-steel autoclave, and kept at 180 °C for 24 h. After cooling to room temperature, the product was collected, washed and dried.	Band gap of 1.76 eV.	[22]
5.	Hydrothermal	A mixture of 60 mL solution containing Bi $(NO_3)_3{\cdot}5H_2O$ (1.815 g), Cu $(NO_3)_2{\cdot}3H_2O$ (0.45 g) and NaOH (0.6525 g) was stirred for 3 h at room temperature. The above mixed solution was poured into 80 mL Teflon-lined steel autoclave and kept in an oven at 180 °C for 24 h. The obtained product was washed with distilled water several times and dried in oven for 12 h at 70 °C. Annealed at 450 °C with a heating rate of 10 °C /min under air atmosphere for 2 h	Smooth rod-like morphology. 200–400 nm in diameter. 1–3 μm in length. Band gap of 1.79 eV.	[23]
6.	Hydrothermal	2.42 g Bi $(NO_3)_3{\bullet}5H_2O$, 0.6 g Cu $(NO_3)_2{\bullet}3H_2O$ was dissolved in 2 mol/L HNO_3. pH was tuned to 11 using 1.25 mol/L NaOH. Mixture solution was poured into the 100 mL autoclave and heated at 180℃ for 24 h. Final product was washed with distilled water and dried at 70 ℃ in a vacuum oven.	Rod-like with diameter of 0.2 μm.	[24]
7.	Hydrothermal	1.2 g of Bi $(NO_3)_3{\cdot}5H_2O$, 0.31 g of Cu $(NO_3)_3{\cdot}3H_2O$, and 0.44 g of NaOH were dissolved in 45 mL of deionized water. The mixture was poured into a 50 mL Teflon-lined autoclave and heated at 180 ℃ for 7 h. Product was washed with H_2O and ethanol five times and dried in an 80 ℃ oven.	$CuBi_2O_4$ shows a rod-shaped structure. Specific surface area of 15 m^2/g. Band gap 1.70 eV.	[11]
8.	Hydrothermal	0.6 g Cu $(NO_3)_2{\cdot}3H_2O$, 2.42 g Bi $(NO_3)_3{\cdot}5H_2O$, and 0.87 g NaOH were mixed into 80 mL deionized water and stirred for 3 h. The mixture was transferred into a 100 mL Teflon-lined stainless-steel autoclave, and then heated at 180 °C for 24 h. Powder was centrifuged and washed for several times with deionized water and absolute ethanol, and then dried at 80 °C for 12 h.	1D microrods structure with a length of *ca.* 2–4 μm and diameter of *ca.* 200–500 nm.	[25]
9.	Hydrothermal	0.9701 g Bi $(NO_3)_3{\cdot}5H_2O$ was dissolved in 5 mL acetic acid. 0.2416 g Cu $(NO_3)_2{\cdot}3H_2O$ was dissolved in 25 mL ethyl alcohol. The two solutions were mixed and NaOH solution was added under magnetic stirring at room temperature until pH 14 was reached. The mixture was transferred into a 100 mL Teflon-lined steel autoclave, and then maintained in an oven at 120 °C for various time durations. The obtained products were washed with ethanol and distilled water three times and then dried in a vacuum drying oven for 12 h at 80 °C.	The band gap $CuBi_2O_4$ synthesized in 15 min hydrothermal treatment duration could hardly be determined. The $CuBi_2O_4$ synthesized in 30 min hydrothermal treatment duration had a band gap of 1.75 eV.	[26]
10.	Hydrothermal	Bi $(NO_3)_3{\cdot}5H_2O$ (1.358 g), Cu $(NO_3)_3{\cdot}3H_2O$ (0.668 g) and NaOH (1.68 g) were dissolved in distilled water (70 mL) and constantly stirred for 3 h. The above was transferred into a 100 mL steel autoclave and heated for 24 h at 180 °C. The precipitate was washed with distilled water, and dried at 60 °C for 12 h.	Band gap of 1.76 eV. A rod-like structure with a length in the range of 2–6 μm and an average diameter of about 200 nm.	[27]
11.	Hydrothermal	Cu $(NO_3)_3{\cdot}3H_2O$ (0.60 g), NaOH (0.87 g), and Bi $(NO_3)_3{\cdot}5H_2O$ (2.42 g) were placed in 80 mL of distilled water to obtain a mixed solution and stirred magnetically for 3 h. The mixture was poured into a 150 mL Teflon-lined steel autoclave and heated at 180 °C for 24 h. The product was cooled to ambient temperature, and washed four times with DI water. Dried in oven at 60 °C for 10 h.	Rod-like morphology. Band gap of 1.76 eV.	[28]
12.	Hydrothermal	60 mL mixture containing NaOH (0.02 mol), Cu $(NO_3)_2{\cdot}3H_2O$ (0.002 mol) and Bi $(NO_3)_3{\cdot}5H_2O$ (0.004 mol) was stirred for 3 h. The mixture was poured into an 80 mL Teflon-lined steel autoclave and heated at 180 °C for 24 h. Deionized water and ethanol were used to wash the produced samples several times and dried at 70 °C for 12 h.	Nanorods with diameter of about 500 nm. Specific surface area of 4.3 m^2/g. Band gap of 1.79 eV.	[29]
13.	Hydrothermal	2.42 g of Bi $(NO_3)_3{\cdot}5H_2O$, 0.60 g of Cu $(NO_3)_2{\cdot}3H_2O$ and 0.87 g of NaOH were added into 80 mL deionized water and stirred at room temperature for 3 h. The above mixed solution was transferred into Teflon-lined stainless-steel autoclave, heated at 180 °C in the oven for 24 h, and cooled down. The product was washed several times alternatively with deionized water and ethanol. Sample was dried in a vacuum oven at 70 °C overnight.	Rod-like structure with approximately 1 μm in length and approximately 200 nm in diameter. Band gap of 1.74 eV.	[30]
14.	Hydrothermal	Bi $(NO_3)_3{\cdot}5H_2O$ solution (20 mL, 0.04 mol/L) and Cu $(NO_3)_2{\cdot}3H_2O$ solution (20 mL, 0.02 mol/L) were mixed by magnetic stirring for 30min. NaOH solution (20 mL, 1.2 mol/L) was added into the above clear solution. The mixed solution was transferred into a sealed Teflon-lined autoclave and heated at 180 °C for 24 h. After cooling to room temperature, the product was washed and dried.	Band gap of 1.77 eV	[31]

No.	Method	Reaction conditions	Feature(s)	Ref.
15.	Hydrothermal	0.04 M $Bi(NO_3)_3 \cdot 5H_2O$ was initially dissolved into 3 mL HNO_3 under the acute agitation. 20 mL of $Cu(NO_3)_2 \cdot 3H_2O$ (0.02 M) was then mixed with the above solution and mechanically agitated for 30 min. After addition of 20 mL NaOH (1.2 M) in dropwise, the mixture was diluted to 70 mL and then transferred into a 100-mL sealed Teflon-lined stainless-steel autoclave for 24 h at 100 °C. The autoclave was cooled naturally to room temperature, the precipitate was isolated by centrifugation and washed several times with distilled water. Dried at 60 °C overnight.	Band gap of 1.72 eV.	[32]
16.	Hydrothermal	1 mmol of $Cu(NO_3)_2 \cdot 3H_2O$ was completely dissolved in 25 mL of distilled water under vigorous magnetic stirring for 30 min. 2 mmol of $Bi(NO_3)_2 \cdot 5H_2O$ was slowly added to this solution and continuously stirred for another 30 min. 25 ml of NaOH (2 M) was added dropwise to the above solution to attain pH 14. Suspension was transferred to Teflon-lined stainless-steel autoclave, sealed and maintained at 180 °C for 10 h. Cooled to room temperature, centrifuged and powder was washed several times with the deionized water, and then dried at 100 °C for 1 h in the oven.	Sphere-shape morphology consisting of individual plate-like nanostructures. Band gap of 1.7 eV.	[33]
17.	Hydrothermal	80 mL solution containing $Bi(NO_3)_3 \cdot 5H_2O$ (0.9201 g), $Cu(NO_3)_2 \cdot 3H_2O$ (0.2416 g) and HNO_3 (20 mL) was stirred for 2 h at room temperature. pH was adjusted to 12 using NaOH. The mixed solution was poured into a 100 mL Teflon-lined steel autoclave and kept in an oven at 180 °C for 12 h. Obtained product was washed with distilled water several times. Dried in oven for 12 h at 60 °C.	Band gap of 1.84 eV. BET surface area of 6.4736 eV.	[34]
18.	Hydrothermal	$Cu(NO_3)_2 \cdot 3H_2O$ and $Bi(NO_3)_2 \cdot 5H_2O$ were weighed with a molar ratio of 1:2 and added to 50 mL 0.5 mol/L nitric acid solution. The mixture was dissolved completely by magnetic stirring. 2 M NaOH was slowly added to regulate the pH to 12.64. The mixture was stirred for 1 h to form a blue suspension. The mixture was kept in drying oven at 200 °C for 2 h. Rinsed 5 times with alcohol and deionized water. Dried in an oven at 85 °C for 12 h.	Spherical shape with diameter of 3 – 6 μm. Band gap of 1.65 eV.	[35]
19.	Hydrothermal	0.0030 M $Bi(NO_3)_3 \cdot 5H_2O$ was dissolved in 30 mL of double distilled water containing 1 mL HNO_3, and stirred at room temperature for 30 min. 0.5 g of a surfactant (sodium dodecyl sulfate) was used. 0.0016 M of $Cu(CH_3COO)\,2.H_2O$ added dropwise in 30 mL of water under constant magnetic stirring for 30 min. 2 M NaOH was slowly dropped into the reaction solution till it reached the pH above 10. Poured into 100 mL Teflon lined autoclave and kept in a hot air oven at 120 °C for 12 h. Precipitate cooled, centrifuged and washed with distilled water and ethanol several times. Dried in hot air oven.	Spherical shaped particles with different diameters. Band gap of 1.43 eV.	[36]
20	Hydrothermal	1 mmol of $Cu(NO_3)_2 \cdot 3H_2O$ and 2 mmol of $Bi(NO_3)_3 \cdot 5H_2O$ were mixed into 30 mL of absolute ethanol and 5 mL of acetic acid. $Bi(NO_3)_3 \cdot 5H_2O$ solution was dropped into $Cu(NO_3)_2 \cdot 3H_2O$ solution and stirred for 10 min. 2M NaOH was gradually dropped into the above mixture and the pH value of the solution was adjusted to 14. The mixture was poured into 100 mL polytetrafluoroethylene autoclave, and maintained at 120 °C for 1.5 h. Centrifuged, rinsed several times with deionized water and absolute ethanol. Dried at 60 °C overnight.	Specific surface area of 4.02 m^2/g. Band gap of 1.61 eV.	[37]
21.	Hydrothermal	0.025 M of $Bi(NO_3)_3 \cdot 5H_2O$ and 0.061 M of $(CH_3COO)_2Cu \cdot H_2O$ were dissolved in the ethanol–water mixture (80 mL) with the volume ratio of ethanol and water $V_{ethanol}:V_{water}$ = 1:1. NaOH solution was added to adjust pH of the above solution under stirring until a dark blue suspension was formed. The suspension remained stirring for another 30 min in an inner tube for autoclave. The autoclave with inter tube was sealed and maintained at 120 °C for 12 h. After the autoclave was cooled down to room temperature, products were collected by centrifugation, washed for 5 times with distilled water and absolute ethanol, and then dried at 80 °C for 8 h.	Nanoparticles with size of 50 – 100 nm.	[19]
22.	Microwave-assisted hydrothermal	20 mL of a 0.03 M solution of $Bi(NO_3)_3 \cdot 5H_2O$, 3 mL of HNO_3 and 20 mL of 0.015 M solution of $Cu(NO_3)_2 \cdot 3H_2O$ under constant magnetic stirring until complete solubilization. 60 mL of 1.25 M solution of NaOH was added to the capsule which was then autoclaved. The microwave treatment was performed at 100 °C for 32 min. Product cooled naturally to room temperature, recovered by centrifugation, washed twice in water, and then dried in air at 60 °C for 12 h.	Band gap of 1.80 eV	[17]
23.	Co-precipitation	2 mmol of $Cu(NO_3)_2 \cdot 3H_2O$, 4 mmol of $Bi(NO_3)_3 \cdot 5H_2O$ and 5 mmol of KCl were successively dissolved in 20 mL of dilute nitric acid solution	Dumbbell-like architecture built from nanorods. Absorption edge at 657.4 nm.	[12]

No.	Method	Reaction conditions	Feature(s)	Ref.
		(2 mL HNO_3 + 18 mL distilled water) to form a uniform mixture solution. 9.6 g of NaOH dissolved in 60 mL of distilled water was then dropped slowly into the above mixture solution under constant stirring, during which time a suspension was immediately formed. The suspension was magnetically stirred for another 12 h at a temperature of 15 °C. The produced precipitate was collected and washed with distilled water (3 times) and ethanol (2 times), followed by drying at 60 °C for 12 h.		
24.	Co-precipitation	0.05 M Bi $(NO_3)_3 \cdot 5H_2O$ and 0.05 M Cu $(NO_3)_2 \cdot 3H_2O$ was prepared in a 50 mL HNO_3. 2 M NaOH was gradually added drop by drop to the mixed solution while stirring continuously, resulting in the immediate formation of a suspension solution. A brown precipitate gradually formed during continuous magnetic stirring of the suspension for 10 h at room temperature. The collected precipitate was washed with distilled water and ethanol, and then dried in hot air oven at 100 °C for 2 h. Product was obtained after calcining the gel at 600 °C for 3 h.	Surface area of 4.3272 m^2/g. Band gap of 2.9 eV.	[38]
25.	Solid-state	1.552 g of Bi $(NO_3)_3 \cdot 5H_2O$, 0.3866 g of Cu $(NO_3)_2 \cdot 3H_2O$ and 1.92 g of NaOH were mixed together. This was followed by a ball-milling reaction for 2 h at room temperature using the planetary ball-mill (QM-3SP04) at the rotation speed of 480 rpm. The resulting product was washed with deionized water and absolute ethanol for several times, and then dried under vacuum at 60 °C for 8 h.	Band gap of 1.56 eV.	[15]
26.	Pechini	1 mol of citric acid was dissolved in 4 mol of ethylene glycol with constant stirring at room temperature for 24 h to obtain a transparent solution. 0.0333 mol of copper (II) chloride dihydrate and 0.0667 mol of bismuth (III) chloride were dissolved in the solution and stirred at 90 °C for 5 h to form a metal−citric acid complex through a chelating process. The solution was then stirred at 140 °C for another 16 h for polyesterification. The polymeric product was decomposed to a black powder via pyrolysis at 400 °C for 5 h in air, and then it was grounded. Calcination was performed between 500 and 700 °C for 6 h at heating rate of 5 °C/min.	Calcination at higher temperature results in an increase in the particle size. Increase in calcination resulted in a decrease in surface area. A decrease in the band gap energies with increase in the calcination temperature was observed.	[5]
27.	polyacrylamide gel route	0.01 mol of Bi $(NO_3)_3 \cdot 5H_2O$ and 0.005 mol of Cu $(NO_3)_2 \cdot 3H_2O$ were dissolved in 30 mL of dilute nitric acid solution. 0.0225 mol of tartaric acid, 20 g of glucose, and 0.135 mol of acrylamide were successively added to the above solution, under continuous magnetic stirring. The above solution was made up to 100 mL by adding distilled water, and then heated up to 80 °C and maintained at this temperature on a hot plate for 3 h. The formed gel was dried at 120 °C for 12 h in a thermostatic drier, and the obtained xerogel was grounded in a mortar. Calcined at 600 °C for 10 h in a tubular furnace.	Average particle size of 550 nm. BET specific surface area of 12.4 m^2/g. Band gap of 1.89 eV.	[2]
28.	Mechanochemical	Grinding Bi_2O_3 and CuO at 1:1 molar ratio using a ball mill (Pulversitte-7, Fritsch, Germany) in an air atmosphere with a ZrO_2 milling vessel (45 cm^3 inner volume) and ZrO_2 balls (7 pieces of 15 mm in diameter). Milling speed of 600 rpm, and the milling time of 2 h.	Band gap of 1.48 eV	[4]
29.	Electrochemical	DMSO solution containing 20 mM Bi $(NO_3)_3 \cdot 5H_2O$, 10 mM Cu $(NO_3)_2 \cdot 2.5H_2O$, and 100 mM $KClO_4$ was used as the plating solution. Deposition was carried out by passing 0.04 C/cm^2 at E = −1.5 V vs Ag/AgCl, followed by resting time of 2 s. This cycle was repeated 10 times to pass a total charge of 0.40 C/cm^2. Cu/Bi films were heated at 450 °C for 3 h in air (ramping rate = 3.5 °C/min) to form $CuBi_2O_4$ films.	Band gap of ~ 1.8 eV.	[7]
30.	Drop-casting	Bi $(NO_3)_3 \cdot 5H_2O$ was dissolved in acetic acid at a concentration of 0.1 M. Cu $(NO_3)_2 \cdot 3H_2O$ was dissolved in ethanol at 0.0125 M. 1 part 0.1 M Bi $(NO_3)_3 \cdot 5H_2O$ in acetic acid mixed with 4 parts 0.0125 M $Cu(NO_3)_2 \cdot 3H_2O$. 25 $\mu L/cm^2$ (substrate area) of the precursor solution was drop-cast onto a substrate lying flat in a muffle furnace under ambient conditions. Immediately after drop-casting the furnace was heated to 60 °C with a ramp rate of 5 °C/min and held for 1 h. It was subsequently heated to 450 °C with a ramp rate of 10 °C/min and held for 2 h. Drop-casting was repeated using same procedure to increase film thickness.	Reticulated nanostructure consisting of open windows and struts.	[6]

3. Applications of $CuBi_2O_4$

3.1. As a photocatalyst

In the field of organic pollutants degradation, $CuBi_2O_4$ has attracted significant attention due its tetragonal spinel structure and excellent spectral response range [39]. Furthermore, the photocatalytic performance of $CuBi_2O_4$ has been enhanced by co-catalyst deposition, exploring material morphology, and formation of heterojunctions with other semiconductors or structure doping [40]. The studies reporting the application of $CuBi_2O_4$ -based photocatalysts to degrade organic pollutants are quite significant (Table 2). Muankaew et al. [38] synthesized $CuBi_2O_4$ via co-precipitation and microwave-assisted for the photocatalytic

degradation of malachite green dye. Due its flower-like morphology and large surface area, the performance by the $CuBi_2O_4$ synthesized via microwave assisted is higher than the photocatalytic performance of $CuBi_2O_4$ synthesized via co-precipitation. In some cases, such as in the study by Xie et al. [16] and Chen et al. [41], the photocatalytic performance of $CuBi_2O_4$ towards degradation of pollutants was tested in the presence of H_2O_2. There was also a unique approach by Cao et al. [42] to enhance the visible light driven photocatalytic activity of $CuBi_2O_4$ through its piezoelectric response. Following bi-harvesting of photo- and vibration energies, 98.1% Rhodamine B (RhB) was degraded, which is higher than ~38.7% degraded as a result of single photocatalysis and ~72.8% degraded due to single piezocatalysis. Such enhanced performance by $CuBi_2O_4$ is attributed to the intensified separation of charge carriers under the piezoelectric potential.

Besides photocatalytic degradation of organic pollutants in wastewater, the inactivation of pathogenic and harmful microorganisms is another issue receiving significant attention. There is a study by Shi et al. [24] involving the photocatalytic disinfection of Escherichia coli (E. coli) using $CuBi_2O_4$. Although the performance displayed by pristine $CuBi_2O_4$ is limited, however, the use of $CuBi_2O_4$ /Bi_2MoO_6 resulted in an enhanced performance. The mechanism of photocatalytic disinfection towards E. coli of $CuBi_2O_4$ /Bi_2MoO_6 heterojunctions was attributed to the cell-membrane disruption, leakage and damage of cellular content including total protein and DNA. Similarly, Liu et al. [11] reported the photocatalytic inactivation of Escherichia coli (E. coli) and Staphylococcus aureus (S. aureus) using $CuBi_2O_4$. Moreover, Zhou et al. [43] also reported the photocatalytic degradation of gaseous benzene using $CuBi_2O_4$.

There was a study by Arai et al. [44] involving the oxidation of acetaldehyde into CO_2 over $CuBi_2O_4$/WO_3 photocatalyst. Although, no CO_2 generation was observed over the pristine $CuBi_2O_4$ catalyst and the CO_2 generation over WO_3 is minimal, however, there was complete photooxidation of acetaldehyde (ca. 9000 ppm) into CO_2 (ca. 18 000 ppm) within 3 h by $CuBi_2O_4$ /WO_3. The use of $CuBi_2O_4$ photocatalyst for the selective oxidation of benzyl alcohol has also been reported [37]. In addition, the use of $CuBi_2O_4$ for the photoreduction of CO_2 has been reported by Ribeiro et al. [17], and approximately 90% in the conversion of CO_2 to CH_4 was achieved. In a different study, Lahmar et al. [45] reported the use of $CuBi_2O_4$ for the photocatalytic reduction of chromate. Although, the reduction was minimal in the presence of pristine $CuBi_2O_4$, however, 98% reduction was achieved for 30 mg/L 〖HCrO〗_4^- in less than 4 h at pH ~4 using optimised $CuBi_2O_4$ /TiO_2 heterosystem.

3.2. As a photocathode material

The use of $CuBi_2O_4$ as a photocathode material for photoelectrochemical water splitting owing to its positive flat band potential vs the reversible hydrogen electrode and extended visible-light absorption has been reported [3]. The process involves using a device immersed in an electrolyte under light illumination to produce hydrogen and oxygen. Berglund et al. [6] reported the use of $CuBi_2O_4$ as a photocathode material for photoelectrochemical water splitting. In addition, Hahn et al. [46] also reported the electrochemical synthesis of P- $CuBi_2O_4$ for the photoelectrochemical hydrogen production. However, they observed that electronic properties of P- $CuBi_2O_4$ needs to be improved using more efficient thin film synthesis techniques and/or doping to produce a more viable P- $CuBi_2O_4$ ¬ for the photoelectrochemical hydrogen production from water. Besides hydrogen production, Sun et al. [47] reported the use of $CuBi_2O_4$ photocathode with integrated electric field for H_2O_2 production. The synergy of photothermoelectricity and photoelectricity resulted in enhanced H_2O_2 production, 2.4 times higher than $CuBi_2O_4$.

Table 2
Photocatalytic degradations of organic pollutants using pristine and coupled $CuBi_2O_4$ photocatalysts.

Catalyst	Pollutant	Light source	Concentration	Degradation/Time (%/min)		Ref.
				$CuBi_2O_4$	Coupling system	
$AgI/CuBi_2O_4$	Tetracycline	Visible	10 mg/L	29/60 min	80/60 min	[9]
$AgBr/CuBi_2O_4$	Tetracycline	Visible	10 mg/L	29/60 min	90/60min	[9]
$CuBi_2O_4/NaTaO_3$	Methylene blue	Visible	20 mg/L	< 10/100 min	>95/100 min	[20]
$CuBi_2O_4/CuO$	Methylene blue	Solar irradiation	30 mg/L	8/60 min	18.3/60 min	[40]
$BiOCl/CuBi_2O_4$	Diclofenac	Visible	50 mg/L	3/60 min	90/60 min	[21]
$CQDs/CuBi_2O_4$	Rhodamine B	Simulated sunlight	5 mg/L	85.6/60 min	90.6/60 min	[12]
$Ag\text{-}CuBi_2O_4$	Rhodamine B	Simulated sunlight	2 mg/L	74.2/60 min	91.7/60 min	[2]
$Ag\text{-}CuBi_2O_4$	Phenol	Simulated sunlight	2 mg/L	62.8/60 min	79.4/60 min	[2]
$N\text{-}BiOBr/CuBi_2O_4$	Tetracycline	Visible	20 mg/L	20/60 min	94%/60 min	[39]
$CuBi_2O_4/MoS_2$	Tetracycline	Visible	10 mg/L	36/120 min	76/120 min	[22]
$CuBi_2O_4/Bi_2MoO_6$	Tetracycline	Visible	20 mg/L	9.2/60 min	72.8/60 min	[48]
$CuBi_2O_4/Bi_2MoO_6$	Oxytetracycline	Visible	20 mg/L	< 10/60 min	74/60 min	[48]
$CuBi_2O_4/Bi_2MoO_6$	Chlortetracycline	Visible	20 mg/L	< 10/60 min	74.4/60 min	[48]
$CuBi_2O_4/Bi_2MoO_6$	Ciprofloxacin	Visible	20 mg/L	< 10/60 min	36.7/60 min	[48]
$Bi_2WO_6/CuBi_2O_4$	Tetracycline	Visible	15 mg/L	44/60 min	94/60 min	[23]
$Ag_3PO_4/CuBi_2O_4$	Tetracycline	Visible	10 mg/L	45/60 min	~75/60 min	[49]
$CuBi_2O_4/Bi_4O_5I_2$	Tetracycline	LED	20 mg/L	9.78/90 min	81.67/90 min	[11]
$CuBi_2O_4/CoV_2O_6$	Tetracycline	Visible	20 mg/L	9.2/120 min	77/120 min	[25]
$CuBi_2O_4$	Methylene blue	Visible	0.02 mM	91/30 min	-	[26]
$Bi_2MoO_6/CuBi_2O_4$	Ciprofloxacin	Visible	10 mg/L	25.8/180 min	90.2/180 min	[50]
$CuBi_2O_4$/polyaniline	Ammonia	LED	30 mg/L	70/180 min	96/180 min	[51]
$Au/CuBi_2O_4$	Tetracycline	Visible	10 mg/L	52/120 min	93/120 min	[27]
$Ag\text{-}CuBi_2O_4$	Methyl orange	Visible	1×10^{-5} mol dm^{-3}	49.61/80 min	66.43/80 min	[52]
$Ag\text{-}CuBi_2O_4$	Methylene blue	Visible	1×10^{-5} mol dm^{-3}	54.55/80 min	65.89/80 min	[52]
$CuBi_2O_4/In_2O_3$	Methylene blue	Visible	10 mg/L	66/80 min	97/80 min	[28]
$CuBi_2O_4/Bi_2WO_6$	Tetracycline	Visible	20 mg/L	36/120 min	93/120 min	[53]
$CuBi_2O_4/Bi_2WO_6$	Ciprofloxacin	Visible	10 mg/L	26/180 min	>90/180 min	[4]
$RGO/CuBi_2O_4$	Methylene blue	Visible	10 mg/L	45/70 min	95/70 min	[54]
$RGO/CuBi_2O_4$	Methyl orange	Visible	10 mg/L	40/100 min	87/100 min	[54]
$BiPO_4/CuBi_2O_4$	Tetracycline	Simulated sunlight	40 mg/L	33.1/90 min	87.5/90 min	[30]
$Bi_2O_3/CuBi_2O_4$	17-α Ethinylestradiol	Visible	10 mg/L	21/120 min	74.3/120 min	[55]
$Bi_2O_2CO_3/CuBi_2O_4$	Malachite green	Simulated sunlight	200 mg/L	68/180 min	91.6/180 min	[56]
$CuBi_2O_4$	Diclofenac	Visible	10 mg/L	67.12/120 min	-	[32]
$CoTiO_3/CuBi_2O_4$	Direct red 16	LED	5 mg/L	~55/90 min	91/90 min	[33]

3.3. Gas-sensing applications

The use of $CuBi_2O_4$ for the sensing of various reducing gases (C_2H_5OH, NH_3, H_2, CO, and H_2S) and oxidizing gas (NO_2) has been reported by Choi *et al.* [5]. The gas-response and sensor resistance characteristics were found to be dominantly affected by the concentration of intrinsic defect in $CuBi_2O_4$. Interestingly, $CuBi_2O_4$ sensor with the 500 °C calcined powder showed the highest gas responses with the highest defect concentration. Also, Xu *et al.* [57] reported the use of $CuBi_2O_4$ in the sensing of formaldehyde, methanol, ethanol and ammonia gases.

3.4. Activation of peroxymonosulfate (PMS) / peroxydisulfate (PDS)

The sulfate radical ($SO_4^{\bullet-}$) based advanced oxidation processes has been effective in remediating wastewater polluted by varieties of organic pollutants. Compared to $^{\bullet}OH$, the $SO_4^{\bullet-}$ has a longer half-life (30 – 40 µs), higher redox potential (2.5 – 3.1 V versus SHE, depending on pH), higher selectivity and wider use [58, 59]. In addition, under neutral or alkaline conditions, the $SO_4^{\bullet-}$ can be converted to $^{\bullet}OH$ thereby expanding wastewater remediation scope of PS/PMS [60]. The $SO_4^{\bullet-}$ is usually generated through activation of persulfate (PS, $S_2O_8^{2-}$) or peroxymonosulfate (PMS, HSO_5^-) via auxiliary methods such as photochemical, thermolysis, transition metal ions, carbon materials etc. [61]. Zhang *et al.* [62] conducted a study involving the use of $CuBi_2O_4$ as a photoactivator of PMS for degradation of antibiotics. The degradation efficiency towards ceftiofur by $CuBi_2O_4$/PMS was around 20%, while that of $CuBi_2O_4$/light/PMS was more than 60%, indicating that $CuBi_2O_4$ is an effective photoactivator for PMS.

In a different study, Oh *et al.* [63] conducted a study on hierarchically-structured Co-$CuBi_2O_4$ and Cu–$CuBi_2O_4$ for sulfanilamide removal *via* peroxymonosulfate activation. They found that catalyst loading was the secondary factor influencing the degradation compared to Oxone® dosage in the case of Cu–$CuBi_2O_4$/PMS. However, a reverse trend was observed in the case of Co–$CuBi_2O_4$/PMS, an indication that Co–$CuBi_2O_4$ is a better catalyst for the activation of PMS than Cu–$CuBi_2O_4$. Besides PMS, Sabri *et al.* [64] reported the use of $CuBi_2O_4$ in the persulfate-assisted photocatalytic degradation of dyes. Peng *et al.* [65] and Wang *et al.* [66] reported peroxydisulfate activation over a $CuBi_2O_4$ catalyst for degradation of organic pollutants.

3.5. For use in electrochemical sensors

Nowadays, due to their simplicity, versatility, and fast response features, electrochemical sensors represent the main category of sensors. Although carbon-based sensors are frequently used in this regard, nevertheless, the rate of electron transfer at the carbon surface is slow. Dumitru *et al.* [67] reported the use of $CuBi_2O_4$ in sensitive amperometric/voltammetric detection of amoxicillin in aqueous solutions. Also, Gudipati *et al.* [68] reported the electrochemical detection of 4-nitrophenol on nanostructured $CuBi_2O_4$.

3.6. Others

Another potential application of $CuBi_2O_4$ is to activate H2O2 by serving as a Fenton catalyst. The Fenton reaction is famous among the advanced oxidation processes (AOPs) used in waste water remediation. For instance, Liu et al. [69] reported the use of $CuBi_2O_4$ as catalyst for the removal of ciprofloxacin in photo-electro-Fenton-like system. Similarly, Cheng and Wang [70] reported the use of $CuBi_2O_4$ as anode material as a high-capacity and cycle-stable anode material for Li recharge batteries. Due to the short diffusion length of Li ions in the 2-dimensional structure, the as-prepared sample delivered a higher capacity, outstanding cycling stability, and high-rate capability. All these are indications that the sample could replace commercial graphite anodes in Li-ion batteries

4. Conclusion

$CuBi_2O_4$ is a p-type semiconductor and a unique representative of the spinel-type compounds. Based on the survey of recent literature, various methods including hydrothermal, co-precipitation, microwave-assisted, mechanochemical, solid-state etc. have effectively been used to synthesize $CuBi_2O_4$ of different morphologies, particle sizes, band gaps, surface areas etc. The material was found to be promising and has effectively been used in the field of photocatalysis, gas sensing, photoelectrochemical water splitting, activating peroxymonosulfate/peroxydisulfate etc. to fulfil various demands. Although, the present study is expected to facilitate the growth of research interest in $CuBi_2O_4$, nevertheless, future researchers are encouraged examine the toxicity and also explore more potential applications of $CuBi_2O_4$.

Author contributions

Saifullahi Shehu Imam: Conceptualization and Writing – Original Draft Preparation. Data Collection, Data Analysis, and Visualization. Investigation, Supervision, and Writing – Review & Editing.

Funding

No funding was received for this study.

Conflict of interest

The authors declare no conflict of interest.

Data availability

No data is available.

REFERENCES

[1] N. Henry, O. Mentre, J. Boivin, F. Abraham, Local Perturbation in Bi2CuO4: Hydrothermal Synthesis, Crystal Structure, and Characterization of the New Bi2 (Cu1-2 x M x) O4 (M= Bi, Pb), Chemistry of materials, 13 (2001) 543-551.
[2] F. Wang, H. Yang, Y. Zhang, Enhanced photocatalytic performance of CuBi2O4 particles decorated with Ag nanowires, Materials Science in Semiconductor Processing, 73 (2018) 58-66.
[3] F.E. Oropeza, N.Y. Dzade, A. Pons-Martí, Z. Yang, K.H. Zhang, N.H. De Leeuw, E.J. Hensen, J.P. Hofmann, Electronic structure and interface energetics of CuBi2O4 photoelectrodes, The Journal of Physical Chemistry C, 124 (2020) 22416-22425.
[4] Z. Li, M. Chen, Q. Zhang, D. Tao, Mechanochemical synthesis of a Z-scheme Bi2WO6/CuBi2O4 heterojunction and its visible-light photocatalytic degradation of ciprofloxacin, Journal of Alloys and Compounds, 845 (2020) 156291.
[5] Y.-H. Choi, D.-H. Kim, S.-H. Hong, CuBi2O4 prepared by the polymerized complex method for gas-sensing applications, ACS applied materials & interfaces, 10 (2018) 14901-14913.
[6] S.P. Berglund, F.F. Abdi, P. Bogdanoff, A. Chemseddine, D. Friedrich, R. Van De Krol, Comprehensive evaluation of CuBi2O4 as a photocathode material for photoelectrochemical water splitting, Chemistry of Materials, 28 (2016) 4231-4242.
[7] D. Kang, J.C. Hill, Y. Park, K.-S. Choi, Photoelectrochemical properties and photostabilities of high surface area CuBi2O4 and Ag-doped CuBi2O4 photocathodes, Chemistry of Materials, 28 (2016) 4331-4340.

[8] F. Wang, W. Septina, A. Chemseddine, F.F. Abdi, D. Friedrich, P. Bogdanoff, R. Van De Krol, S.D. Tilley, S.P. Berglund, Gradient self-doped CuBi2O4 with highly improved charge separation efficiency, Journal of the American Chemical Society, 139 (2017) 15094-15103.
[9] F. Guo, W. Shi, H. Wang, M. Han, W. Guan, H. Huang, Y. Liu, Z. Kang, Study on highly enhanced photocatalytic tetracycline degradation of type II AgI/CuBi2O4 and Z-scheme AgBr/CuBi2O4 heterojunction photocatalysts, Journal of hazardous materials, 349 (2018) 111-118.
[10] G. Sharma, Z. Zhao, P. Sarker, B.A. Nail, J. Wang, M.N. Huda, F.E. Osterloh, Electronic structure, photovoltage, and photocatalytic hydrogen evolution with p-CuBi 2 O 4 nanocrystals, Journal of Materials Chemistry A, 4 (2016) 2936-2942.
[11] J. Liu, L. Huang, Y. Li, J. Yao, S. Shu, L. Huang, Y. Song, Q. Tian, Constructing an S-scheme CuBi2O4/Bi4O5I2 heterojunction for light emitting diode-driven pollutant degradation and bacterial inactivation, Journal of Colloid and Interface Science, 621 (2022) 295-310.
[12] H. Gao, F. Wang, S. Wang, X. Wang, Z. Yi, H. Yang, Photocatalytic activity tuning in a novel Ag2S/CQDs/CuBi2O4 composite: Synthesis and photocatalytic mechanism, Materials Research Bulletin, 115 (2019) 140-149.
[13] H. Yin, M.-L. Cao, X.-X. Yu, C. Li, Y. Shen, M.-Q. Zhu, Hierarchical CuBi 2 O 4 microspheres as lithium-ion battery anodes with superior high-temperature electrochemical performance, RSC advances, 7 (2017) 13250-13256.
[14] Y.-H. Choi, D.-H. Kim, S.-H. Hong, Gas sensing properties of p-type CuBi2O4 porous nanoparticulate thin film prepared by solution process based on metal-organic decomposition, Sensors and Actuators B: Chemical, 268 (2018) 129-135.
[15] M. Chen, Q. Yang, L. Li, M. Liu, P. Xiao, M. Zhang, Solid-state synthesis of CuBi2O4/MWCNT composites with enhanced photocatalytic activity under visible light irradiation, Materials Letters, 171 (2016) 255-258.
[16] Y. Xie, Y. Zhang, G. Yang, C. Liu, J. Wang, Hydrothermal synthesis of CuBi2O4 nanosheets and their photocatalytic behavior under visible light irradiation, Materials letters, 107 (2013) 291-294.
[17] L.S. Ribeiro, I.M. Pinatti, J.A. Torres, A.S. Giroto, F. Lesse, E. Longo, C. Ribeiro, A.E. Nogueira, Rapid microwave-assisted hydrothermal synthesis of CuBi2O4 and its application for the artificial photosynthesis, Materials Letters, 275 (2020) 128165.
[18] X. Zhang, S. Wang, L. Lin, X. Tan, Y. Zeng, Design of a novel CuBi2O4/CdMoO4 heterojunctions with nano-microsphere structure: Synthesis and photocatalytic degradation mechanism, Colloids and Surfaces A: Physicochemical and Engineering Aspects, 614 (2021) 126008.
[19] A. Abdulkarem, J. Li, A. Aref, L. Ren, E. Elssfah, H. Wang, Y. Ge, Y. Yu, CuBi2O4 single crystal nanorods prepared by hydrothermal method: Growth mechanism and optical properties, Materials Research Bulletin, 46 (2011) 1443-1450.
[20] Y. Deng, Y. Chen, B. Chen, J. Ma, Preparation, characterization and photocatalytic activity of CuBi2O4/NaTaO3 coupled photocatalysts, Journal of alloys and compounds, 559 (2013) 116-122.
[21] S. Wu, X. Yu, J. Zhang, Y. Zhang, Y. Zhu, M. Zhu, Construction of BiOCl/CuBi2O4 S-scheme heterojunction with oxygen vacancy for enhanced photocatalytic diclofenac degradation and nitric oxide removal, Chemical Engineering Journal, 411 (2021) 128555.
[22] F. Guo, M. Li, H. Ren, X. Huang, W. Hou, C. Wang, W. Shi, C. Lu, Fabrication of pn CuBi2O4/MoS2 heterojunction with nanosheets-on-microrods structure for enhanced photocatalytic activity towards tetracycline degradation, Applied Surface Science, 491 (2019) 88-94.
[23] X. Yuan, D. Shen, Q. Zhang, H. Zou, Z. Liu, F. Peng, Z-scheme Bi2WO6/CuBi2O4 heterojunction mediated by interfacial electric field for efficient visible-light photocatalytic degradation of tetracycline, Chemical Engineering Journal, 369 (2019) 292-301.
[24] H. Shi, J. Fan, Y. Zhao, X. Hu, X. Zhang, Z. Tang, Visible light driven CuBi2O4/Bi2MoO6 pn heterojunction with enhanced photocatalytic inactivation of E. coli and mechanism insight, Journal of hazardous materials, 381 (2020) 121006.
[25] J. Luo, X. Zhou, F. Yang, X. Ning, L. Zhan, Z. Wu, X. Zhou, Generating a captivating S-scheme CuBi2O4/CoV2O6 heterojunction with boosted charge spatial separation for efficiently removing tetracycline antibiotic from wastewater, Journal of Cleaner Production, 357 (2022) 131992.
[26] Y. Wang, F. Cai, P. Guo, Y. Lei, Q. Xi, F. Wang, Short-time hydrothermal synthesis of CuBi2O4 nanocolumn arrays for efficient visible-light photocatalysis, Nanomaterials, 9 (2019) 1257.
[27] W. Shi, M. Li, H. Ren, F. Guo, X. Huang, Y. Shi, Y. Tang, Construction of a 0D/1D composite based on Au nanoparticles/CuBi2O4 microrods for efficient visible-light-driven photocatalytic activity, Beilstein Journal of Nanotechnology, 10 (2019) 1360-1367.
[28] C. Fang, H. Su, M. Hu, Z. Jiang, L. Xu, C. Liu, Construction and performance of a novel CuBi2O4/In2O3 Z-scheme heterojunction photocatalyst, Materials Science in Semiconductor Processing, 160 (2023) 107464.
[29] N. Li, H. Du, M. Tan, L. Yang, B. Xue, S. Zheng, Q. Wang, Construction of Z-scheme CuBi2O4/MIL-88A (Fe) heterojunctions with enhanced LED light driven photocatalytic Cr (VI) reduction and antibacterial performance, Applied Surface Science, 614 (2023) 156249.
[30] C. Lu, L. Wang, D. Yang, Z. Jin, X. Wang, J. Xu, Z. Li, W. Shi, W. Guan, W. Huang, Boosted tetracycline and Cr (VI) simultaneous cleanup over Z-Scheme BiPO4/CuBi2O4 pn heterojunction with 0D/1D trepang-like structure under simulated sunlight irradiation, Journal of Alloys and Compounds, 919 (2022) 165849.
[31] J.-X. Mao, J.-C. Wang, H. Gao, W. Shi, H.-P. Jiang, Y. Hou, R. Li, W. Zhang, L. Liu, S-scheme heterojunction of CuBi2O4 supported Na doped P25 for enhanced photocatalytic H2 evolution, International Journal of Hydrogen Energy, 47 (2022) 8214-8223.
[32] X. Chen, Y. Dai, J. Guo, Hydrothermal synthesis of well-distributed spherical CuBi2O4 with enhanced photocatalytic activity under visible light irradiation, Materials Letters, 161 (2015) 251-254.
[33] H. Ramezanalizadeh, E. Rafiee, Design, fabrication, electro-and photoelectrochemical investigations of novel CoTiO3/CuBi2O4 heterojunction semiconductor: An efficient photocatalyst for the degradation of DR16 dye, Materials Science in Semiconductor Processing, 113 (2020) 105055.
[34] K. Song, C. Zhang, Y. Zhang, G. Yu, M. Zhang, Y. Zhang, L. Qiao, M. Liu, N. Yin, Y. Zhao, Efficient tetracycline degradation under visible light irradiation using CuBi2O4/ZnFe2O4 type II heterojunction photocatalyst based on two spinel oxides, Journal of Photochemistry and Photobiology A: Chemistry, 433 (2022) 114122.
[35] Z. Zhang, H. Hao, H. Yang, L. Zhu, C. Ding, G. Zhang, J. Bi, S. Yan, G. Liu, H. Hou, UV-Vis-NIR-light-driven Ag2O/Ag2S/CuBi2O4 double Z-scheme configuration for enhanced photocatalytic applications, Materials Science in Semiconductor Processing, 126 (2021) 105668.
[36] P. Annamalai, D. Thangavelu, M. Ramadoss, S. Subramani, S.P. Muthu, R. Perumalsamy, S. Ranganathan, V. Hector, Electrochemical sensing of tyrosine and removal of toxic dye using self-assembled three-dimensional CuBi2O4/rGO microsphere composite, Colloid and Interface Science Communications, 45 (2021) 100523.
[37] Z. Zhang, X. Hao, S. Hao, J. Li, Preparation of Pd@ CuBi2O4 photocatalysts and their performance for selective oxidation of benzyl alcohol under visible light illumination, Materials Science in Semiconductor Processing, 142 (2022) 106499.
[38] R. Muankaew, C. Banphot, P. Thammaacheep, P. Jannoey, W. Khanitchaidecha, A. Nakaruk, D. Channei, Synthesis of Flower-Like CuBi2O4 Microspheres and Its Photocatalytic Activity, Trends in Sciences, 21 (2024) 7200-7200.
[39] T. Ma, H. Long, Z. Shi, Z. Lang, M. Zhao, S. Zhang, C. Lei, Efficient photocatalytic degradation of TC under visible light with three-dimensional flower shaped N doped BiOBr/CuBi2O4, Optical Materials, 143 (2023) 114175.
[40] A.C. Nogueira, L.E. Gomes, J.A. Ferencz, J.E. Rodrigues, R.V. Goncalves, H. Wender, Improved visible light photoactivity of CuBi2O4/CuO heterojunctions for photodegradation of methylene blue and metronidazole, The Journal of Physical Chemistry C, 123 (2019) 25680-25690.
[41] X. Chen, N. Li, S. Xu, H. Wang, Y. Cai, Study on the visible-light photocatalytic performance and degradation mechanism of diclofenac sodium under the system of hetero-structural CuBi2O4/Ag3PO4 with H2O2, Materials, 11 (2018) 511.
[42] Y. Cao, T. He, M. Li, Z. Cao, Y. Gao, J. Liu, G. Li, A novel strategy to enhance the visible light driven photocatalytic activity of CuBi2O4 through its piezoelectric response, Journal of Physics and Chemistry of Solids, 167 (2022) 110732.
[43] Y. Zhou, H. Deng, Z. Li, Y. Wang, T. Ma, Construction of CuBi2O4/BiOBr/Biochar Z-Scheme Heterojunction for Degradation of Gaseous Benzene Under Visible Light, Catalysis Letters, 153 (2023) 2319-2330.
[44] T. Arai, M. Yanagida, Y. Konishi, Y. Iwasaki, H. Sugihara, K. Sayama, Efficient complete oxidation of acetaldehyde into CO2 over CuBi2O4/WO3 composite photocatalyst under visible and UV light irradiation, The Journal of Physical Chemistry C, 111 (2007) 7574-7577.
[45] H. Lahmar, M. Benamira, F. Akika, M. Trari, Reduction of chromium (VI) on the hetero-system CuBi2O4/TiO2 under solar light, Journal of Physics and Chemistry of Solids, 110 (2017) 254-259.
[46] N.T. Hahn, V.C. Holmberg, B.A. Korgel, C.B. Mullins, Electrochemical synthesis and characterization of p-CuBi2O4 thin film photocathodes, The Journal of Physical Chemistry C, 116 (2012) 6459-6466.
[47] M. Sun, B. Liu, W. Han, Z. Zhang, M. Xie, CuBi2O4 photocathode with integrated electric field for enhanced H2O2 production, Applied Catalysis B: Environmental, 304 (2022) 120980.
[48] W. Shi, M. Li, X. Huang, H. Ren, F. Guo, Y. Tang, C. Lu, Construction of CuBi2O4/Bi2MoO6 pn heterojunction with nanosheets-on-microrods structure for improved photocatalytic activity towards broad-spectrum antibiotics degradation, Chemical Engineering Journal, 394 (2020) 125009.
[49] W. Shi, F. Guo, S. Yuan, In situ synthesis of Z-scheme Ag3PO4/CuBi2O4 photocatalysts and enhanced photocatalytic performance for the degradation of tetracycline under visible light irradiation, Applied Catalysis B: Environmental, 209 (2017) 720-728.
[50] Z. Li, R. Zheng, S. Dai, T. Zhao, M. Chen, Q. Zhang, In-situ mechanochemical fabrication of pn Bi2MoO6/CuBi2O4 heterojunctions with efficient visible light photocatalytic performance, Journal of Alloys and Compounds, 882 (2021) 160681.

[51] N. Ahmad, J. Anae, M.Z. Khan, S. Sabir, P. Campo, F. Coulon, A novel CuBi2O4/polyaniline composite as an efficient photocatalyst for ammonia degradation, Heliyon, 8 (2022).
[52] V. Dutta, A. Sudhaik, P. Raizada, A. Singh, T. Ahamad, S. Thakur, Q. Van Le, V.-H. Nguyen, P. Singh, Tailoring S-scheme-based carbon nanotubes (CNTs) mediated Ag-CuBi2O4/Bi2S3 nanomaterials for photocatalytic dyes degradation in the aqueous system, Journal of Materials Science & Technology, 162 (2023) 11-24.
[53] L. Wang, G. Yang, D. Wang, C. Lu, W. Guan, Y. Li, J. Deng, J. Crittenden, Fabrication of the flower-flake-like CuBi2O4/Bi2WO6 heterostructure as efficient visible-light driven photocatalysts: Performance, kinetics and mechanism insight, Applied Surface Science, 495 (2019) 143521.
[54] A. Muthukrishnaraj, S. Vadivel, I.M. Joni, N. Balasubramanian, Development of reduced graphene oxide/CuBi2O4 hybrid for enhanced photocatalytic behavior under visible light irradiation, Ceramics International, 41 (2015) 6164-6168.
[55] D. Majhi, A.K. Mishra, K. Das, R. Bariki, B. Mishra, Plasmonic Ag nanoparticle decorated Bi2O3/CuBi2O4 photocatalyst for expeditious degradation of 17α-ethinylestradiol and Cr (VI) reduction: Insight into electron transfer mechanism and enhanced photocatalytic activity, Chemical Engineering Journal, 413 (2021) 127506.
[56] A. Sokhansanj, M. Haghighi, M. Shabani, Macroporous flowerlike Bi2O2CO3-CuBi2O4 nanoheterojunction photocatalyst for high concentrated malachite green degradation: influence of nanocomposite composition and sonication approach, Journal of Molecular Liquids, 371 (2023) 121024.
[57] J. Xu, H. Zhang, Z. Fu, Y. Ling, Hydrothermal synthesis of hierarchical CuBi2O4 microspheres with improved gas sensitivity, Ceramics International, 48 (2022) 31519-31527.
[58] J. Yao, Y. Zhang, Z. Dong, Enhanced degradation of contaminants of emerging concern by electrochemically activated peroxymonosulfate: Performance, mechanism, and influencing factors, Chemical Engineering Journal, 415 (2021) 128938.
[59] X. Xu, R. Lin, X. Deng, J. Liu, In situ synthesis of FeOOH-coated trimanganese tetroxide composites catalyst for enhanced degradation of sulfamethoxazole by peroxymonosulfate activation, Separation and Purification Technology, 275 (2021) 119184.
[60] C. Wang, J. Zhao, C. Chen, P. Na, Catalytic activation of PS/PMS over Fe-Co bimetallic oxides for phenol oxidation under alkaline conditions, Applied Surface Science, 562 (2021) 150134.
[61] F. Chen, G.-X. Huang, F.-B. Yao, Q. Yang, Y.-M. Zheng, Q.-B. Zhao, H.-Q. Yu, Catalytic degradation of ciprofloxacin by a visible-light-assisted peroxymonosulfate activation system: Performance and mechanism, Water research, 173 (2020) 115559.
[62] H. Zhang, L.-c. Nengzi, X. Li, Z. Wang, B. Li, L. Liu, X. Cheng, Construction of CuBi2O4/MnO2 composite as Z-scheme photoactivator of peroxymonosulfate for degradation of antibiotics, Chemical Engineering Journal, 386 (2020) 124011.
[63] W.-D. Oh, Z. Dong, T.-T. Lim, Hierarchically-structured Co–CuBi2O4 and Cu–CuBi2O4 for sulfanilamide removal via peroxymonosulfate activation, Catalysis Today, 280 (2017) 2-7.
[64] M. Sabri, A. Habibi-Yangjeh, S. Ghosh, Novel ZnO/CuBi2O4 heterostructures for persulfate-assisted photocatalytic degradation of dye contaminants under visible light, Journal of Photochemistry and Photobiology A: Chemistry, 391 (2020) 112397.
[65] C. Peng, X. Chen, Y. Yang, F. Luo, X. He, Y. Yu, Q. Deng, T. Hu, S. Shan, Y. Zhi, Enhanced catalytic performance of peroxydisulfate activation for Rhodamine B degradation over a novel MIL-68 (Fe)/CuBi2O4 catalyst, Journal of Molecular Liquids, 392 (2023) 123476.
[66] X. Wang, N. Su, X. Wang, D. Cao, C. Xu, X. Wang, Q. Yan, C. Lu, H. Zhao, Fabrication of 0D/1D S-scheme CoO-CuBi2O4 heterojunction for efficient photocatalytic degradation of tetracycline by activating peroxydisulfate and product risk assessment, Journal of Colloid and Interface Science, (2024).
[67] R. Dumitru, S. Negrea, C. Păcurariu, A. Surdu, A. Ianculescu, A. Pop, F. Manea, CuBi2O4 synthesis, characterization, and application in sensitive amperometric/voltammetric detection of amoxicillin in aqueous solutions, Nanomaterials, 11 (2021) 740.
[68] N.S. Gudipati, S. Vanjari, S. Korutla, R.R. Tammineni, S. Challapalli, Electrochemical detection of 4-nitrophenol on nanostructured CuBi2O4 with plausible mechanism supported by DFT calculations, Journal of Environmental Chemical Engineering, 10 (2022) 108758.
[69] Y. Liu, W. Yang, Y. Li, S. Wang, S. Zhan, Fabrication of CuBi2O4/Bi2MoO6 pn heterojunction as synergistic photoelectric catalyst for efficient removal of ciprofloxacin in photo-electro-Fenton-like system, Journal of Water Process Engineering, 52 (2023) 103534.
[70] C. Cheng, X. Wang, Preparation of CuBi2O4 nanosheets as a high-capacity and cycle-stable anode material for Li recharge batteries, Journal of Energy Storage, 93 (2024) 112217.